The PTW microSilicon diode: Performance in small 6 and 15 MV photon fields and utility of density compensation

Georgios Georgiou[*†1,2,3], Sudhir Kumar[4], Jan U. Würfel[5], Martyn Gilmore[2], Tracy S. A. Underwood[6], Carl G. Rowbottom[2,3] and John D. Fenwick[1,2]

1. Department of Molecular and Clinical Cancer Medicine, Institute of Systems, Molecular and Integrative Biology, University of Liverpool, The Sherrington Building, Ashton Street, Liverpool L69 3BX, UK

2. Department of Physics, Clatterbridge Cancer Centre, Clatterbridge Road, Wirral CH63 4JY, UK

3. Department of Physics, University of Liverpool, Oliver Lodge Laboratory, Oxford Street, Liverpool L69 7ZE, UK

4. Radiological Physics and Advisory Division, Bhabha Atomic Research Centre, CT & CRS Building, Anushaktinagar, Mumbai-400094, India

5. PTW-Freiburg, Loerracher Str. 7, 79115, Freiburg, Germany

6. Division of Cancer Sciences, School of Medical Sciences, Faculty of Biology, Medicine and Health, The University of Manchester, Manchester M20 4BX, UK

Running title – Response of the PTW microSilicon diode in small fields

[†] Corresponding author, email: geogeorgph@gmail.com

[*]Now at Radiotherapy Physics Department, North Wales Cancer Treatment Centre, Glan Clwyd Hospital, Bodelwyddan LL18 5UJ, UK

Abstract

Purpose: We have experimentally and computationally characterized the PTW *microSilicon* 60023-type diode's performance in 6 and 15 MV photon fields $\geq 5\times 5$ mm^2 projected to isocentre. We tested the detector on- and off-axis at 5 and 15 cm depths in water, and investigated whether its response could be improved by including within it a thin airgap.

Methods: Experimentally, detector readings were taken in fields generated by a Varian TrueBeam linac and compared with doses-to-water measured using Gafchromic film and ionization chambers. An unmodified 60023-type diode was tested along with detectors modified to include 0.6, 0.8 and 1.0 mm thick airgaps. Computationally, doses absorbed by water and detectors' sensitive volumes were calculated using the EGSnrc/BEAMnrc Monte Carlo radiation transport code. Detector response was characterized using $k_{Q_{clin,4\text{ cm}}}^{f_{clin},4\text{ cm}}$, a factor that corrects for differences in the ratio of dose-to-water to detector reading between small fields and the reference condition, in this study 5 cm deep on-axis in a 4×4 cm^2 field.

Results: The greatest errors in measurements of small field doses made using uncorrected readings from the unmodified 60023-type detector were over-responses of 2.6% ± 0.5% and 5.3% ± 2.0% determined computationally and experimentally, relative to the reading-per-dose in the reference field. Corresponding largest errors for the earlier 60017-type detector were 11.9% ± 0.6% and 11.7% ± 1.4% over-responses. Adding even the thinnest, 0.6 mm, airgap to the 60023-type detector over-corrected it, leading to under-responses of up to 4.8% ± 0.6% and 5.0% ± 1.8% determined computationally and experimentally. Further Monte Carlo calculations indicate that a detector with a 0.3 mm airgap would read correctly to within 1.3% on-axis. The ratio of doses at 15 and 5 cm depths in water in a 6 MV 4×4 cm^2 field was measured more accurately using the unmodified 60023-type detector than using the 60017-type detector, and was within 0.3% of the ratio measured using an ion chamber. The 60023-type diode's sensitivity also varied negligibly as dose-rate was reduced from 13 to 4 Gy min^{-1} by decreasing the linac pulse repetition frequency, whereas the sensitivity of the 60017-type detector fell by 1.5%.

Conclusions: The 60023-type detector performed well in small fields across a wide range of beam energies, field sizes, depths and off-axis positions. Its response can potentially be further improved by adding a thin, 0.3 mm, airgap.

Key words: microSilicon, diode, small field, density compensation, dose-rate

1. INTRODUCTION

Detectors used to measure radiation doses absorbed by water from small megavoltage photon fields should ideally have sensitive volumes narrow enough to minimize volume-averaging, and be built from materials with atomic numbers and densities sufficiently close to water to minimize variations in photon spectral effects and electron fluence perturbation with field-size.[1] Sensitive volumes of silicon diode detectors typically have a 1 mm diameter, and silicon's atomic number is close enough to water to limit spectral effects in small fields, especially when an intermediate field, for example 4×4 cm^2, is used as a reference rather than the standard 10×10 cm^2 field. Nevertheless, diodes over-respond in small fields relative to wider ones due largely to the non-water equivalent densities of silicon (2.33 g cm^{-3}) and other detector constituents in close proximity to the sensitive volume.[2-5]

Several 'density compensation' studies have found that silicon diodes' responses in small fields can be improved by building into them airgaps of judiciously chosen size.[4, 6-9] We previously tested an unmodified PTW 60017-type diode (Diode E) (PTW-Freiburg, Germany) and diodes with airgaps of thickness 0.6-1.6 mm added.[10] Density compensation substantially improved diode performance on- and off-axis at depths of 5 and 15 cm in water in 6 and 15 MV photon fields of size ≥0.5×0.5 cm^2. The maximum error in doses measured using uncorrected readings of the unmodified detector was 11.7% determined experimentally or 11.9% computationally, compared to 4.1% or 2.2% for the best performing diode, which had a 1.6 mm airgap.

For some detectors there were notable differences between responses determined experimentally and computationally in 0.5×0.5 cm^2 fields, a finding attributed to detector-to-detector variations in the thickness of the dense epoxy resin housing of the sensitive volume.[10] This was supported by Monte Carlo calculations showing that the response of the 60017-type detector in a 6 MV 0.5×0.5 cm^2 field relative to that in a 4×4 cm^2 field would be 4% higher if the epoxy housing was 0.3 mm thicker, a change within manufacturing tolerance. It follows that detector response in small fields can only be reproducibly fine-tuned using airgaps engineered to a tenth of a millimeter if comparable tolerances are placed on the dimensions of dense detector components, or if these components are replaced with less dense materials.

We also observed experimentally that the response of the 60017-type detector relative to a PTW 31010-type *Semiflex* ionization chamber fell progressively, by up to 2%, at increasing depths in water.[10] This is most likely due to the variation of silicon diode sensitivity with dose-per-linac-pulse observed by Schönfeld et al.[11]

Recently, PTW-Freiburg commercialized a new '*microSilicon*' diode detector, the 60023-type. Some materials used in this detector have densities closer to 1 g cm^{-3}, and the sensitive silicon lattice has been adjusted to minimize the diode's dose-rate dependence. The 60023-type diode has been tested in 6 MV fields ≥0.5×0.5 cm^2 by Schönfeld et al.[11] and Weber et al.[12], who characterized its response on-axis at 10 cm depth in water and off-axis at 5 cm depth. Compared to the 60017-type diode, the new detector required small field correction factors closer to unity. Akino et al.[13] further tested this detector at 10 cm depth in water, on-axis in 6 and 10 MV fields ≥0.5×0.5 cm^2 and off-axis in a 6 MV 1×1 cm^2 field. These investigators also found that correction factors were closer to unity for the 60023-type than for the 60017-type diode, and reported negligible variation in the sensitivity of the new detector across a 0.07-10 Gy min^{-1} range of dose-rates, whereas the sensitivity of the 60017-type detector changed by over 5%. The 60023-type detector has also been tested in a 6 MV circular field of diameter 5 mm by Francescon et al.[14] who found that the on-axis dose measured at 1.5 cm depth required a 2% correction compared to 5-6% for other stereotactic diodes. Wiedlich et al.[15] tested the detector in 3 MV circular fields down to a diameter of 4 mm and reported that the penumbra width measured using this detector was greater than that measured using film or a PTW 60018-type diode, but narrower than the width measured using a *microDiamond* detector, reflecting the relative diameters of the detectors' sensitive volumes.

Here, we describe our own experimental and computational testing of the 60023-type diode in 6 and 15 MV photon beams, on- and off-axis at 5 and 15 cm depths in water, and on-axis from the surface to depths up to 30 cm. To investigate the utility of density-compensation we have additionally tested 60023-type diodes with airgaps added.

2. METHODS

2.A. PTW 60023-type microSilicon detectors

An unmodified 60023-type diode was tested along with variants containing airgaps of thickness 0.6, 0.8 and 1.0 mm. The outer casings of the detectors included RW3 plastic caps.[12] Airgaps were built directly into these caps in modified diodes, keeping the thickness of RW3 above the airgaps equal to that in the unmodified detector.

The sensitive volume of the 60023-type diode is a silicon disc of diameter 1.4 mm and thickness 18 μm, whose short-axis is aligned with the long-axis of the detector. It is located at the upper surface of a thicker silicon cuboid which is surrounded by an epoxy housing located immediately below the RW3 cap or airgap. The manufacturer-specified effective point of measurement (EPOM) of the unmodified PTW 60023-type diode lies 0.9 mm below the detector's top surface, slightly higher than in the 60017-type which has denser epoxy.

2.B. Characterizing detector response

Response in small clinical fields f_{clin} of quality Q_{clin} was characterized relative to the response at a reference point in a reference field, which in this study was a point on-axis at 5 cm depth in a 4×4 cm^2 field. The difference in response between the two points was accounted for via a standard correction factor, $k_{Q_{clin},4\text{ cm}}^{f_{clin},4\text{ cm}}$, given by the ratio of doses absorbed by water at the measurement and reference points, divided by the ratio of readings (M) of a detector with its EPOM located at those points[1, 16]

$$k_{Q_{clin},4\text{ cm}}^{f_{clin},4\text{ cm}} = \left[\frac{\left(D_{w-point}\right)_{Q_{clin}}^{f_{clin}} \Big/ M_{Q_{clin}}^{f_{clin}}}{\left(D_{w-point}\right)_{Q_{4\text{ cm}}}^{4\text{ cm}} \Big/ M_{Q_{4\text{ cm}}}^{4\text{ cm}}}\right] \tag{1}$$

2.C. Monte Carlo calculations

Radiation transport calculations were performed using the EGSnrc system (version: v20017)[17] run on a 64 core AMD 6378 Opteron-based computer. Phase-space files were generated for linac jaw-defined fields of size 0.5×0.5, 0.7×0.7 and 4×4 cm^2 projected to isocentre, using the BEAMnrc user-code[18] and 6 and 15 MV beam models previously built and validated for Varian Clinac iX and 2100 C treatment machines by Underwood et al.[19] and Scott et al.[20] For the phase-space calculations the electron and photon cut-off parameters ECUT and PCUT were set to 700 and 10 keV respectively. Electrons with total energies below 700 keV travel <0.5 mm in water[21] while low energy photons comprise a small part of the energy spectra of linac photon beams[22-23] and those with energies below 10 keV typically travel <0.5 cm through water before interacting.[24]

2.C.1. <u>In-water doses</u>

The DOSXYZnrc code (version: v20017)[25] was used to calculate doses absorbed from 6 and 15 MV fields by water voxels within a 50×50×50 cm^3 water phantom located at 100 cm source-to-surface distance (SSD). Radiation transport parameters were selected as described previously, with ECUT and PCUT set to 521 and 1 keV[10], electrons and photons with lower energies typically travelling <10 μm through water before stopping or interacting.[21, 24]

On-axis doses were calculated at 5 and 15 cm depths in water for the three fields. Off-axis dose-in-water profiles were calculated for the 0.5×0.5 cm^2 field at 5 and 15 cm depths, and a percentage depth-dose (PDD) was calculated along the central axis down to 30 cm depth. Water voxel dimensions were chosen to allow doses to be calculated with good statistical precision and suitable spatial resolution in reasonable times, as detailed in Table I. All doses in our Monte Carlo simulations were normalized by numbers of electrons incident on the linac target.

2.C.2. <u>Detector readings</u>

Models of the unmodified 60023-type detector and the detector with a 0.6 mm airgap added were built *in-silico* according to the manufacturer's blueprints, using the EGS++ geometry package within the egs_chamber user-code (version: v20017).[26] Some Monte Carlo calculations were also run for a 60023-type detector with a 0.3 mm thick airgap, although a real detector with an airgap of this thickness has yet to be manufactured. PEGS4 data-files containing detector material cross-section and stopping-power data were created as described previously[10], setting the AE and AP thresholds for knock-on electrons and secondary bremsstrahlung photons to 512 and 1 keV respectively.

In-silico, detectors were aligned parallel to the beam and positioned within a $50\times50\times50$ cm^3 water phantom. Doses absorbed by detector sensitive volumes were calculated using the egs_chamber user-code. Detector readings were considered to be proportional to these doses, the proportionality constant cancelling in calculations of relative readings. The global ECUT and PCUT thresholds were set to 521 and 1 keV, electrons and photons with lower energies typically travelling <1.5 and 5 μm respectively through silicon before stopping or interacting.[21, 24] Photon cross-section enhancement was used to accelerate calculations.[10]

Doses absorbed by detector sensitive volumes located on-axis at 5 and 15 cm depths in water in 6 and 15 MV fields of size 0.5×0.5, 0.7×0.7 and 4×4 cm^2 were computed to a precision of ≤±0.2% (2 standard deviations, s.d.). To simulate field profiles measured at these depths, sensitive volume doses were calculated for detectors computationally shifted across the 0.5×0.5 cm^2 field in 0.25 mm steps, holding precision to ≤±0.7% up to 1 mm beyond the field-edge. Since the beam and detector models were symmetric, only half-profiles were calculated.

PDD curves measured for the 0.5×0.5 cm^2 field were simulated by calculating sensitive volume doses for detectors located on-axis at depths increasing from 0-2 cm in 0.5 mm steps, from 2-5 cm in 1 mm steps, 5-20 cm in 1 cm steps, and 20-30 cm in 5 cm steps. Doses were calculated to a precision of ≤±0.7% up to 15 cm deep, and ≤±1% beyond this depth.

2.D. Experimental measurements

The 60023-type detectors were tested experimentally in a Blue Phantom 2 water tank (IBA dosimetry, Schwarzenbruck, Germany) set up at an SSD of 100 cm. They were placed one-by-one in the tank, aligned parallel to the beam-axis, connected to an electrometer box and associated OmniPro-Accept 7.4 computer software with no bias voltage[10], and irradiated in 6 and 15 MV fields generated by a Varian TrueBeam linear accelerator (linac) (Varian Medical systems, Palo Alta, California) oriented at 0° gantry angle.

Measurements were made for filter-flattened 6 and 15 MV square-fields of nominal side-length 0.5, 0.7, 1.0, 3.0, 4.0, 6.0 and 10.0 cm projected to isocentre, and for an additional filter-flattened 6 MV square-field of side-length 1.5 cm. Fields were collimated using the linac jaws with multieaves retracted. Once set for a particular field and beam energy, jaw positions were maintained until measurements were complete for all detectors. In-line and cross-line profiles were measured at depths of 5 and 15 cm for the 0.5×0.5 and 0.7×0.7 cm^2 fields. In these fields particular care was taken to ensure detectors were centered, adjusting the zeroing of a detector's lateral coordinates if measured profiles were offset by more than 0.3 mm from the origin, limiting possible under-measurement of on-axis doses due to detector mis-positioning to the 1% level.[19] On-axis readings were taken with the diodes positioned at 5 and 15 cm depths in water and irradiated using fixed numbers of monitor units (MUs). Finally, PDD curves were measured down the beam central-axis.

When making the on-axis measurements used to calculate $k_{Q_{clin,4\ \mathrm{cm}}}^{f_{clin},4\ \mathrm{cm}}$ factors, the top surfaces of diodes were positioned 0.9 mm above the intended measurement point, on the assumption that EPOMs in the modified detectors lay 0.9 mm below the detector tops, as for the unmodified 60023-type detector. Small changes in EPOM with airgap thickness will have negligible effect on resulting $k_{Q_{clin,4\ \mathrm{cm}}}^{f_{clin},4\ \mathrm{cm}}$ values, which depend only on ratios of detector measurements.[10] Doses-to-water also form part of the $k_{Q_{clin,4\ \mathrm{cm}}}^{f_{clin},4\ \mathrm{cm}}$ calculation and were measured using EBT3 film for fields ≤1.5×1.5 cm^2 and an IBA CC13 ionization chamber for fields ≥3×3 cm^2.

To determine any dose-rate dependence, unmodified 60023- and 60017-type diodes were placed on-axis at 5 cm depth in a water phantom set up with an SSD of 100 cm, and repeatedly irradiated to 300 MU in a 4×4 cm^2 6 MV flattening-filter-free (FFF) field. The linac's nominal dose-rate was varied right across the range deliverable for this field, from 400 to 1300 MU min^{-1} in increments of 200 MU min^{-1} by changing the pulse repetition frequency. Dose-per-MU was determined at the measurement point using an NE2571A-type ionization chamber, allowing dose-rates to be calculated in Gy min^{-1}. Detector sensitivities were measured as charge-per-Gy and normalized to the sensitivity at 600 MU min^{-1}.

2.E. Radiochromic film techniques

In small fields, measurements of doses absorbed by water were made using 6×6 cm^2 squares of Gafchromic EBT3 film. The squares were handled with nitrile gloves under minimum light, placed one-by-one in a metallic frame, submerged at the measurement depth in water with an SSD of 100 cm and irradiated as previously described.[10]

To generate calibration curves, films placed at 5 cm depth in a 4×4 cm^2 field were irradiated to seven dose-levels ranging from 0 to 4.35 Gy. Five film-squares were irradiated at each dose-level and separate curves were measured for the 6 and 15 MV beams. Doses in small fields were then measured at 5 and 15 cm depths by irradiating three film-squares at each field size and depth combination, scaling MUs so that roughly 2 Gy was delivered to each film.

At 48 hours after irradiation film-squares were scanned using an Epson V750 Pro scanner (Epson UK, Hemel Hempstead). Using in-house software[8] 6 and 15 MV calibration curves were created and dose-maps extracted from scanned films as arrays in which each point represents the average dose in a 0.51×0.51 mm^2 area.[10]

2.F. Uncertainty estimation

Statistical uncertainties estimated history-by-history[27] in Monte Carlo calculated doses were taken from output files, and uncertainties in doses measured using detectors and film were calculated from repeat measurements. Uncertainties in quantities such as detector correction factors and measurement inaccuracy were calculated from these underlying uncertainties using standard error propagation techniques. All uncertainties are shown at the ± 2 s.d. level.

3. RESULTS

3.A. Monte Carlo simulated data

3.A.1. On-axis $k_{Q_{clin,4\ \mathrm{cm}}}^{f_{clin},4\ \mathrm{cm}}$ factors

Table II lists Monte Carlo-calculated on-axis $k_{Q_{clin,4\ \mathrm{cm}}}^{f_{clin},4\ \mathrm{cm}}$ values for detectors irradiated in 6 MV 0.5×0.5 and 0.7×0.7 cm^2 fields at 5 cm depth in water.

For the unmodified 60023-type detector, $k_{Q_{0.5,4\ \mathrm{cm}}}^{0.5,4\ \mathrm{cm}}$ and $k_{Q_{0.7,4\ \mathrm{cm}}}^{0.7,4\ \mathrm{cm}}$ were 0.979 ± 0.006 and 0.977 ± 0.006, indicating small over-responses. For the 60023-type variant with a 0.6 mm airgap corresponding values were 1.029 ± 0.006 and 1.002 ± 0.006, and since these values show that the detector was slightly over-corrected we did not carry out calculations for detectors with 0.8 and 1.0 mm airgaps. For the hypothetical 60023-type variant with a 0.3 mm airgap $k_{Q_{0.5,4\ \mathrm{cm}}}^{0.5,4\ \mathrm{cm}}$ and $k_{Q_{0.7,4\ \mathrm{cm}}}^{0.7,4\ \mathrm{cm}}$ were 1.007 ± 0.006 and 0.995 ± 0.006, better than either the unmodified 60023 detector or its 0.6 mm airgap variant. For comparison, corresponding values previously computed for the 60017-type diode were 0.910 ± 0.005 and 0.971 ± 0.007.[10]

Table II also lists Monte Carlo $k_{Q_{clin,4\text{ cm}}}^{f_{clin},4\text{ cm}}$ values calculated at 15 cm depth in water for 6 MV 0.5×0.5 and 0.7×0.7 cm^2 fields. Results follow the pattern at 5 cm depth: $k_{Q_{clin,4\text{ cm}}}^{f_{clin},4\text{ cm}}$ factors were much closer to unity for the unmodified 60023-type than for the 60017-type diode; the 60023-type detector with the 0.6 mm airgap was over-corrected; and factors calculated for the hypothetical 60023-type detector with the 0.3 mm airgap were closest to unity. The table additionally includes $k_{Q_{clin,4\text{ cm}}}^{f_{clin},4\text{ cm}}$ factors calculated for the 15 MV beam, which follow the same pattern.

<u>3.A.2. Off-axis detector response</u>

Monte Carlo simulations of errors in doses obtained from uncorrected off-axis detector readings are plotted in Fig. 1 for the unmodified 60023-type detector and the 0.6 mm airgap variant. Readings were simulated for detectors located at 5 and 15 cm depths in 6 and 15 MV 0.5×0.5 cm^2 fields, at cross-line positions along the direction of travel of the X jaws. Errors are shown as fractions of on-axis dose.

Within fields the unmodified detector over-responded whereas the detector with the 0.6 mm airgap under-responded. At 5 cm depth in the 6 MV 0.5×0.5 cm^2 field, the maximum error for either detector was ≤3% of the on-axis dose. At 15 cm depth the unmodified detector over-responded by at most 2.1% ± 0.7% normalized to the on-axis dose, and the 0.6 mm airgap detector variant under-responded by at most 4.9% ± 0.7%. In the 15 MV 0.5×0.5 cm^2 field the unmodified detector maximally over-responded by 2.2% and 1.6% ± 0.6% at 5 and 15 cm depths, whereas the 0.6 mm airgap detector maximally under-responded by 4.9% ± 0.5% at both depths.

3.A.3. PDD curves

Monte Carlo PDD data calculated for the 6 MV 0.5×0.5 cm^2 field are shown in Fig. 2. Computed in-water depth-doses are graphed along with simulations of PDDs measured using the unmodified 60023-type detector and the 0.6 mm airgap variant. Figure 2(a) shows the build-up curves: a small lateral offset of 0.2 mm can be seen between the curves calculated for the modified and unmodified diodes. Both curves were plotted so that the 'kick-points' (at which the PDD gradients suddenly increase as the tops of the detectors become submerged[10]) occur at 0.9 mm depth, and thus for the unmodified detector the plotted measurement depths correspond to depths of the manufacturer-specified EPOM.

Figure 2(b) shows whole PDD curves, with the modified detector's PDD now shifted by 0.2 mm. The PDDs simulated for the unmodified and modified diodes agree well and concur with the calculated in-water PDD, both in the build-up region and at greater depths. This is further demonstrated by the ratios of computed diode-measured and in-water PDDs plotted in Fig. 2(c), which between 1 and 30 cm depths in water differ from unity by less than 1%. These results indicate that the EPOM of the modified detector lies 0.9 + 0.2 = 1.1 mm below its top. The same EPOM was obtained when Monte Carlo 15 MV data (not plotted) were analyzed.

3.B. Experimentally measured data

3.B.1. On-axis $k_{Q_{clin,4\ \mathrm{cm}}}^{f_{clin},4\ \mathrm{cm}}$ factors

On-axis $k_{Q_{0.5,4\ \mathrm{cm}}}^{0.5,4\ \mathrm{cm}}$ factors measured experimentally for the unmodified and modified 60023-type detectors at 5 cm depth in water in a 6 MV 0.5×0.5 cm^2 field are plotted in Fig. 3. They increase with airgap thickness from 0.973 ± 0.010 (2 s.d.) for the unmodified

60023-type diode to 1.022, 1.035 and 1.050 ± 0.011 for detectors with airgaps of 0.6, 0.8 and 1.0 mm thickness respectively. Since the diodes with 0.8 mm and 1.0 mm airgaps performed less well than the others, we did not test them further.

On-axis $k_{Q_{clin,4\ \mathrm{cm}}}^{f_{clin},4\ \mathrm{cm}}$ values measured for the unmodified 60023-type detector and the 0.6 mm airgap variant are plotted against field-size in Fig. 4. The factors were measured at 5 and 15 cm depths in water for 6 and 15 MV fields of size 0.5×0.5 to 10×10 cm^2. In the 6 MV small fields the unmodified and modified 60023-type detectors over- and under-responded respectively. Both performed well, though, with $k_{Q_{clin,4\ \mathrm{cm}}}^{f_{clin},4\ \mathrm{cm}}$ lying no further from unity than 2.8% ± 1.0% for the unmodified diode and 3.0% ± 1.2% for the 0.6 mm airgap detector. On-axis $k_{Q_{clin,4\ \mathrm{cm}}}^{f_{clin},4\ \mathrm{cm}}$ values obtained previously for an unmodified 60017-type diode[10] are plotted for comparison and indicate over-responses of up to 8.6% ± 1.1%.

In the 15 MV small fields, the unmodified and modified 60023-type detectors again over- and under-responded by up to 3.6% ± 1.6% and 4.7% ± 1.3% respectively. The 60017-type detector over-responded by at most 10.6% ± 1.4%.

<u>3.B.2. Off-axis detector response</u>

Responses of the unmodified 60023-type detector and the 0.6 mm airgap variant off-axis at 5 and 15 cm depths in 6 and 15 MV 0.5×0.5 cm^2 fields are plotted in Figs. 5 and 6. The plots show profiles of errors in doses obtained from uncorrected detector readings, normalized to the on-axis dose. The errors were calculated from diode and EBT3 film measurements taken cross-line along the direction of travel of the lower (X) jaws.

At 5 cm depth in the 6 MV field, the maximum error for the unmodified 60023-type detector was a 4.0% over-response within the field, normalized to on-axis dose. In comparison the 60017-type detector over-responded by up to 9.7%.[10] For the 0.6 mm airgap detector, maximum errors were a 2.5% under-response within the field and a 3.0% over-response just beyond the field-edge. At 15 cm depth the unmodified 60023-type detector read correctly to within 2.8% of the on-axis dose across most of the measured range, with a maximum 4.0% over-response in a narrow spike attributable to noise in the film profiles. The 0.6 mm airgap detector had a maximum 4.0% under-response.

Similarly, in the 15 MV 0.5×0.5 cm^2 field, maximum errors at depths of 5 and 15 cm were over-responses of 5.3% and 2.9% respectively for the unmodified 60023-type diode, and under-responses of 4.2% and 5.0% for the diode with the 0.6 mm airgap.

3.B.3. PDD curves

Depth-dose curves measured for the 6 MV 0.5×0.5 cm^2 field using the unmodified 60023-type detector and the 0.6 mm airgap variant are plotted in Fig. 7. Build-up curves are shown in Fig. 7(a) with measurement depths plotted so that the kick-points for both detectors occur at 0.9 mm depth. For the unmodified 60023-type diode, plotted measurement depths thus correspond to depths of the EPOM. The longitudinal shift visible between the two build-up curves, 0.2 mm at 80% of the maximum dose, suggests the EPOM of the 0.6 mm airgap diode lies 1.1 mm below its top.

In Fig. 7(b) complete 0.5×0.5 cm^2 PDD curves are plotted for the two detectors, with measurement depths adjusted for the modified diode so that the kick-point of its PDD occurs at 1.1 mm depth. These curves agree well as demonstrated further in Fig. 7(c) in which their ratio is plotted, confirming that the modified detector’s EPOM lies 1.1 mm below its top surface.

Table III lists the ratio of doses measured at 15 and 5 cm depths in the 6 MV 4×4 cm^2 field using the IBA CC13 ionization chamber, which is expected to accurately represent the variation of dose in water with depth. The table also lists equivalent ratios of readings for the 60017-type diode and the unmodified 60023-type detector and its 0.6 mm airgap variant. For the 60017-type detector the ratio was 1.1% ± 0.2% below that measured using the ionization chamber, comparable to a 1% reduction in response of the 60017-type detector relative to an ionization chamber previously observed between 5 and 15 cm depths in measured 4×4 cm^2 PDD curves.[10] For the 60023-type detectors, however, the ratio was only 0.3% ± 0.2% below the ionization chamber ratio.

<u>3.B.4. Dose-rate dependence</u>

Detector sensitivity is plotted against dose-rate in Fig. 8. Across the 4-13 Gy min^{-1} range sensitivity varied by less than 0.1% for the unmodified 60023-type detector compared to 1.5% for the 60017-type detector.

4. DISCUSSION

In 6 and 15 MV small fields ≥0.5×0.5 cm^2, radiation doses can be measured more accurately on- and off-axis at 5 and 15 cm depths in water using uncorrected readings from the new PTW 60023-type *microSilicon* diode than from a 60017-type diode. Monte Carlo calculations show that the 60023-type detector over-responds in the small fields compared to a reference 4×4 cm^2 field by up to 2.6% ± 0.5% and 2.2% ± 0.7% (normalized to on-axis dose-levels) at 6 and 15 MV respectively, whereas earlier calculations for the 60017-type detector indicated over-responses of up to 10.2% ± 0.7% and 11.9% ± 0.6%.[10] Similarly, experimental data show maximum over-responses in small fields of 4.0% ± 1.0% and 5.3% ± 2.0% at 6 and 15 MV for the 60023-type detector, compared to 9.7% ± 1.4% and 11.7% ± 1.4% for the 60017-type detector.

Other investigators have reported that doses in 6 and 10 MV small fields can be measured more accurately at 5 and 10 cm depths in water using 60023-type rather than 60017-type diodes.[11-13] Our results extend these findings up to a beam energy of 15 MV, and to a wider range of detector locations, on- and off-axis at both 5 and 15 cm depths. Our on-axis 6 MV data are in good quantitative agreement with results reported by Schönfeld et al.[11] and Weber et al.[12], who obtained correction factors of 0.960-0.988 for 60023-type detectors positioned at 10 cm depth in water with an SSD of 90 cm and irradiated in 6 MV small fields of size 5.5×5.5 to 6.3×6.3 mm^2, compared to values of 0.973-0.988 reported here for a detector placed on-axis in a 5×5 mm^2 field at 5 and 15 cm depths with an SSD of 100 cm.

The maximum over-responses we measured experimentally for the 60023-type diode were a little higher than those determined computationally. This may be because readings were taken at many off-axis locations, leading to maximum recorded over-responses being recorded at points where results lie at the upper end of uncertainty ranges, which are wider for experimental than for computational results. Closer agreement was seen when only the smaller quantity of on-axis data was considered.

Our off-axis computational and experimental results agreed quite well (Figs. 1, 5, 6). They show the unmodified 60023-type detector slightly over-responding within small fields, and the detector with a 0.6 mm airgap under-responding within these fields but slightly over-responding beyond their edges. The correction factors required vary with detector location as well as field size, and consequently detectors with correction factors that are small and potentially ignorable everywhere are preferable to those requiring a multiplicity of correction factor values to be calculated and applied.

Anomalies in experimental data gathered for 60017-type diodes[10] were not present in data collected for 60023-type diodes. In particular, for 60023-type diodes measured $k_{Q_{clin,4\text{ cm}}}^{f_{clin},4\text{ cm}}$ factors rose monotonically with increasing airgap thickness (Fig. 3), whereas for 60017-type diodes the analogous curve measured had notable inversions at some points.[10] This is likely a consequence of the epoxy housing being less dense in 60023- than in 60017-type detectors, which limits any detector-to-detector response variability resulting from differences in epoxy thickness.

Furthermore, ratios of doses-to-water at 15 and 5 cm depths in a 6 MV 4×4 cm^2 field measured using the unmodified 60023-type detector and its 0.6 mm variant lay within 0.3% of the ratio measured using an IBA CC13 ionization chamber (Table III), whereas the same ratio measured using the 60017-type detector was 1.1% below the ionization chamber ratio. This improved depth-dose accuracy of the 60023-type detector is likely a consequence of its response varying negligibly with the linac dose-per-pulse[11], in turn a result of changes made to its silicon lattice. The 60023-type detector response also varied little with linac pulse repetition frequency (Fig. 8), whereas the 60017-type detector response rose with increasing frequency.

For the 60017-type diode, the best results were achieved by adding a 1.6 mm airgap.[10] For the 60023-type diode the best experimental results we obtained were for a detector with a thin 0.6 mm airgap added, but even this over-corrected the detector. Further Monte Carlo calculations suggest that close-to-optimal results can be obtained using a 60023-type detector with an even thinner 0.3 mm airgap, for which computed under-responses on-axis in 6 and 15 MV 0.5×0.5 cm^2 fields were just 1.0% ± 0.8% in the

6 MV beam and 1.3% ± 0.8% in the 15 MV beam. We have not experimentally characterized such a detector as PTW have yet to fabricate one. The gains achievable in routine practice will depend on the accuracy and precision with which the airgap and other components can be manufactured, and structural stability over time.

Depth-dose data indicate that inclusion of the 0.6 mm thick airgap in the 60023-type detector deepened its EPOM by 0.2 mm from its top surface, in line with a finding in modified 60017-type detectors that EPOM depths were increased by around one-third of airgap thicknesses.[10]

5. CONCLUSIONS

The 60023-type *microSilicon* diode measures radiation doses in small photon fields substantially more accurately than does the 60017-type diode. At 5 and 15 cm depths on- and off-axis in 6 and 15 MV fields $\geq 0.5 \times 0.5$ cm^2, the greatest dosimetric errors found for the 60023-type detector were over-responses of 2.6% ± 0.5% determined computationally and 5.3% ± 2.0% determined experimentally, compared to 11.9% ± 0.6% and 11.7% ± 0.8% for a 60017-type detector. The ratio of doses at 15 and 5 cm depths in a 4×4 cm^2 field was also experimentally measured more accurately using the 60023-type than the 60017-type diode; and whereas the sensitivity of the 60017-type detector fell by 1.5% as dose-rates were reduced from 13 to 4 Gy min^{-1} by decreasing the linac pulse repetition frequency, the sensitivity of the 60023-type detector changed little.

Building a 0.6 mm airgap into the 60023-type diode over-corrected the detector, leading to maximum under-responses in small fields of around 5%. According to further Monte Carlo calculations a 0.3 mm airgap would produce close-to-optimal detector performance.

ACKNOWLEDGEMENTS

The authors thank PTW-Freiburg for manufacturing and providing the diode detectors tested in this work.

CONFLICTS OF INTEREST

Dr Jan U Würfel is an employee of PTW-Freiburg.

DATA AVAIABILITY STATEMENT

The data supporting the findings of this study are presented in the figures and tables.

References

1. Alfonso R, Andreo P, Capote R, et al. Dosimetry of Small Static Fields Used in External Beam Radiotherapy: An International Code of Practice for Reference and Relative Dose Determination. Technical Report Series No. 483. Vienna: International Atomic Energy Agency; 2017.

2. Scott AJD, Kumar S, Nahum AE, Fenwick JD. Characterizing the influence of detector density on dosimeter response in non-equilibrium small photon fields. *Phys Med Biol*. 2012; 57: 4461–4476.

3. Bassinet C, Huet C, Derreumaux S, et al. Small fields output factors measurements and correction factors determination for several detectors for a Cyberknife® and linear accelerators equipped with microMLC and circular cones. *Med Phys.* 2013; 40: 071725.

4. Charles PH, Cranmer-Sargison G, Thwaites DI, Kairn T, Crowe SB, Pedrazzini G, Aland T, Kenny J, Langton CM, Trapp JV. Design and experimental testing of air slab caps which convert commercial electron diodes into dual purpose, correction-free diodes for small field dosimetry. *Med Phys*. 2014; 41: 101701.

5. Fenwick JD, Georgiou G, Rowbottom CG, Underwood TSA, Kumar S, Nahum AE. Origins of the changing detector response in small megavoltage photon radiation fields. *Phys Med Biol*. 2018; 63: 125003.

6. Underwood TSA, Winter HC, Fenwick JD, Hill MA. OC-0512 Modifying detector designs for small field dosimetry. *Radiother Oncol*. 2012; 103: S206.

7. Underwood TSA, Winter HC, Hill MA, Fenwick JD. Mass-density compensation can improve the performance of a range of different detectors under non-equilibrium conditions. *Phys Med Biol*. 2013; 58: 8295–8310.

8. Underwood TSA, Thompson J, Bird L, Scott AJD, Patmore P, Winter HC, Hill MA, Fenwick JD. Validation of a prototype DiodeAir for small field dosimetry. *Phys Med Biol*. 2015; 60: 2939–2953.

9. Charles PH, Crowe SB, Kairn T, Knight RT, Hill B, Kenny J, Langton CM, Trapp JV. Monte Carlo-based diode design for correction-less small field dosimetry. *Phys Med Biol*. 2013; 58: 4501–4512.

10. Georgiou G, Kumar S, Würfel JU, Underwood TSA, Thompson JM, Hill MA, Rowbottom CG, Fenwick JD. Density compensated diodes for small field dosimetry: comprehensive testing and implications for design. *Phys Med Biol*. 2020; 65: 155011.

11. Schönfeld AB, Poppinga D, Kranzer R, De Wilde RL, Willborn K, Poppe B, Looe HK. Technical note: Characterization of the new microSilicon diode detector. *Med Phys*. 2019; 46: 4257-4262.

12. Weber C, Kranzer R, Weidner J, Kröninger K, Poppe B, Looe H, Poppinga D. Small field output correction factors of the microSilicon detector and a deeper understanding of their origin by quantifying perturbation factors. *Med Phys*. 2020; 47: 3165-3173.

13. Akino Y, Fujiwara M, Okamura K, Shiomi H, Mizuno H, Isohashi F, Suzuki O, Seo Y, Tamari K, Ogawa K. Characterization of a microSilicon diode detector for small-field photon beam dosimetry. *J Radiat Res.* 2020; 61: 410-418.

14. Francescon P, Kilby W, Noll JM, Satariano N, Orlandi C. Small field dosimetry correction factors for circular and MLC shaped fields with the CyberKnife M6 System: evaluation of the PTW 60023 microSilicon detector. *Phys Med Biol.* 2020; 65: 01NT01.

15. Weidlich GA, Chung W, Kolli S, Thirunarayan I, Loysel T. Characterization of the ZAP-X peripheral dose fall-off. *Cureus.* 2021; 13: e13972.

16. Alfonso R, Andreo P, Capote R, Huq MS, Kilby W, Kjäll P, Mackie TR, Palmans H, Rosser K, Seuntjens J, Ullrich W, Vatnitsky S. A new formalism for reference dosimetry of small and nonstandard fields. *Med Phys.* 2008; 35: 5179–5186.

17. Kawrakow I, Mainegra-Hing E, Rogers DWO, Tessier F, Walters BRB. The EGSnrc code system: Monte Carlo simulation of electron and photon transport.

Technical Report No. PIRS 701. Ottawa: National Research Council of Canada; 2017.

18. Rogers DWO, Walters B, Kawrakow I. BEAMnrc Users Manual. Technical Report No. PIRS 509 (A) rev L. Ottawa: National Research Council of Canada; 2017.

19. Underwood TSA, Winter HC, Hill MA, Fenwick JD. Detector density and small field dosimetry: integral versus point dose measurement schemes. *Med Phys*. 2013; 40: 082102.

20. Scott AJD, Nahum AE, Fenwick JD. Using a Monte Carlo model to predict dosimetric properties of small radiotherapy photon fields. *Med Phys*. 2008; 35: 4671–4684.

21. National Institute of Science and Technology. Stopping Power and Range Tables for Electrons (https://physics.nist.gov/PhysRefData/Star/Text/ESTAR.html); 2021. (Accessed: 5th July 2021)

22. Ali ESM, Rogers DWO. Functional forms for photon spectra of clinical linacs. *Phys Med Biol.* 2012; 57: 31-50.

23. Khabaz R. Effect of each component of a LINAC therapy head on neutron and photon spectra. *Appl Radiat Isot.* 2018; 139: 40-45.

24. Hubbell JH, Seltzer SM. Tables of X-Ray Mass Attenuation Coefficients and Mass Energy-Absorption Coefficients (Version 1.4). Gaithersburg, MD: National Institute of Standards and Technology; 2004

25. Rogers DWO, Kawrakow I, Seuntjens JP, Walters BRB, Mainegra-Hing E. NRC User Codes for EGSnrc. Technical Report No. PIRS-702 rev C. Ottawa: National Research Council of Canada; 2017.

26. Wulff J, Zink K, Kawrakow I. Efficiency improvements for ion chamber calculations in high energy photon beams. *Med Phys.* 2008; 35: 1328-1336.

27. Walters BRB, Kawrakow I, Rogers DWO. History by history statistical estimators in the BEAM code system. *Med Phys.* 2002; 29: 2745-2752.

FIGURE LEGENDS:

FIG. 1. Monte Carlo calculations of errors in doses obtained from uncorrected detector readings off-axis at 5 and 15 cm depths in water for 6 and 15 MV 0.5×0.5 cm^2 fields, normalized to on-axis doses. Results are plotted for the unmodified 60023-type detector and the 0.6 mm airgap (a.g.) variant. ± 2 s.d. error bars are shown.

FIG. 2. Monte Carlo depth-dose data for a 6 MV 0.5×0.5cm^2 field, showing in-water doses and simulations of PDDs measured using the unmodified 60023-type detector and the 0.6 mm airgap (a.g.) variant: (a) the build-up region; (b) complete PDD curves; (c) ratios of diode-measured to in-water PDD curves, normalized to unity at 5 cm depth. Measurement depths were defined as 0.9 mm below the top surface of both detectors in panel (a), and 0.9 and 1.1 mm below the tops of the unmodified 60023-type diode and the 0.6 mm airgap variant in (b) and (c). Statistical uncertainties on calculated doses were ≤1% (2 s.d.) and are omitted to improve visual clarity.

FIG. 3. On-axis $k_{Q_{0.5,4\text{ cm}}}^{0.5,4\text{ cm}}$ correction factors measured experimentally in a 6 MV beam for unmodified and modified 60023-type detectors at 5 cm depth in water, plotted against airgap thickness. ±2 s.d. error bars are shown.

FIG. 4. On-axis $k_{Q_{clin,4\text{ cm}}}^{f_{clin},4\text{ cm}}$ values measured experimentally in 6 MV and 15 MV square fields at 5 and 15 cm depths in water, for the unmodified 60023-type detector and the 0.6 mm airgap (a.g.) variant. Data for an unmodified 60017-type diode are shown for comparison. The reference condition was on-axis in a 4×4 cm^2 field at 5 cm depth in water. ±2 s.d. error bars are shown.

FIG. 5. Off-axis diode response measured experimentally in a 6 MV 0.5×0.5 cm^2 field for the unmodified 60023-type detector and the 0.6 mm airgap (a.g.) variant. Plots show errors in measured doses across the field at 5 and 15 cm depths in water, obtained from uncorrected detector readings, relative to the on-axis dose. Data for the unmodified 60017-type diode at 5 cm depth are shown for comparison. ±2 s.d. error bars are shown on-axis, at the field-edge and 4.5 mm beyond the field-edge.

FIG. 6. Off-axis diode response measured experimentally in a 15 MV 0.5×0.5 cm^2 field for the unmodified 60023-type detector and the 0.6 mm airgap (a.g.) variant. Data for the unmodified 60017-type diode at 5 cm depth are shown for comparison. ±2 s.d. error bars are shown.

FIG. 7. 6 MV depth-dose data measured experimentally for a 0.5×0.5 cm^2 field using the unmodified 60023-type diode and the 0.6 mm airgap (a.g.) variant, showing (a) the build-up region, (b) complete PDD curves, (c) the ratio of PDD curves. In (a) measured depths are plotted so that the kick-points occur at 0.9 mm for both detectors, whereas in (b) and (c) depths have been shifted for the modified detector so that its kick-point occurs at 1.1 mm depth.

FIG. 8. Sensitivities of the unmodified 60017- and 60023-type detectors, measured experimentally on-axis at 5 cm depth in water in a 6 MV 4×4 cm^2 field. Dose-rate was varied by changing the linac pulse repetition frequency. Results are normalized to the sensitivity at 600 MU min^{-1}.

FIG. 1.

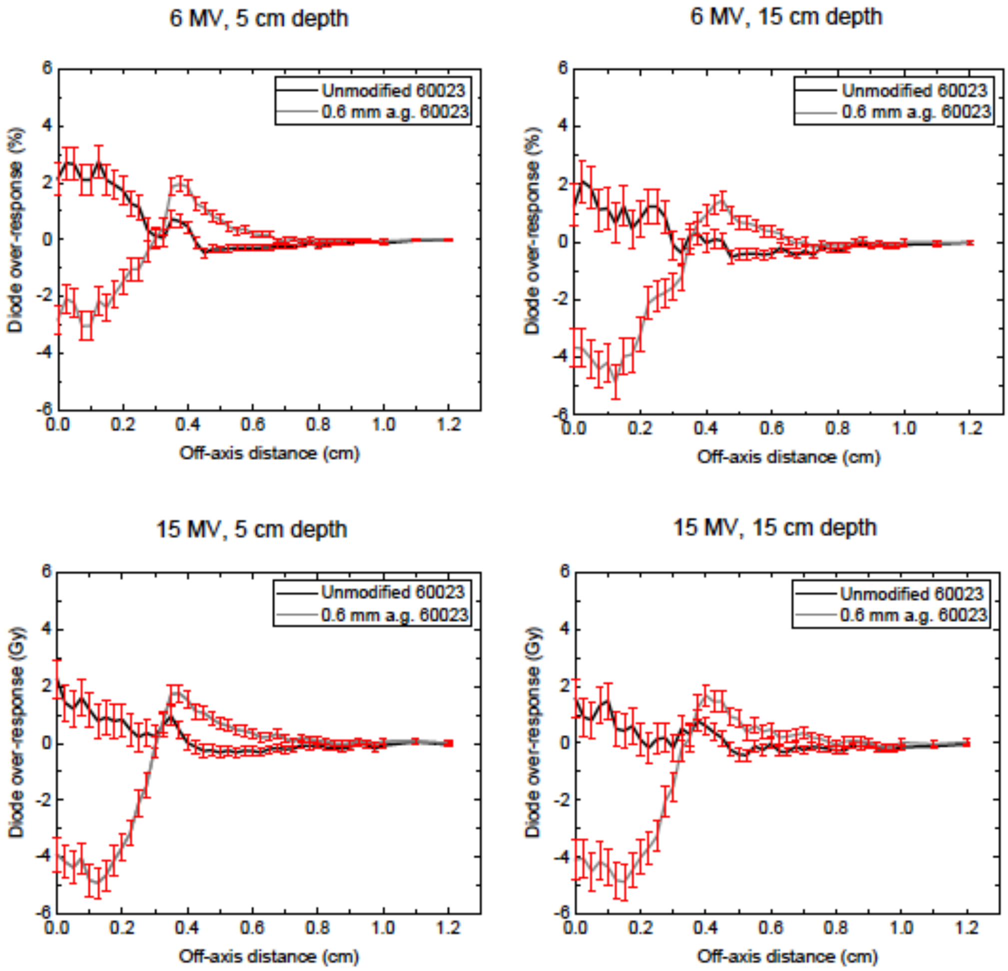
6 MV, 5 cm depth
6 MV, 15 cm depth
15 MV, 5 cm depth
15 MV, 15 cm depth
Unmodified 60023
0.6 mm a.g. 60023
Diode over-response (%)
Diode over-response (Gy)
Off-axis distance (cm)

FIG. 2.

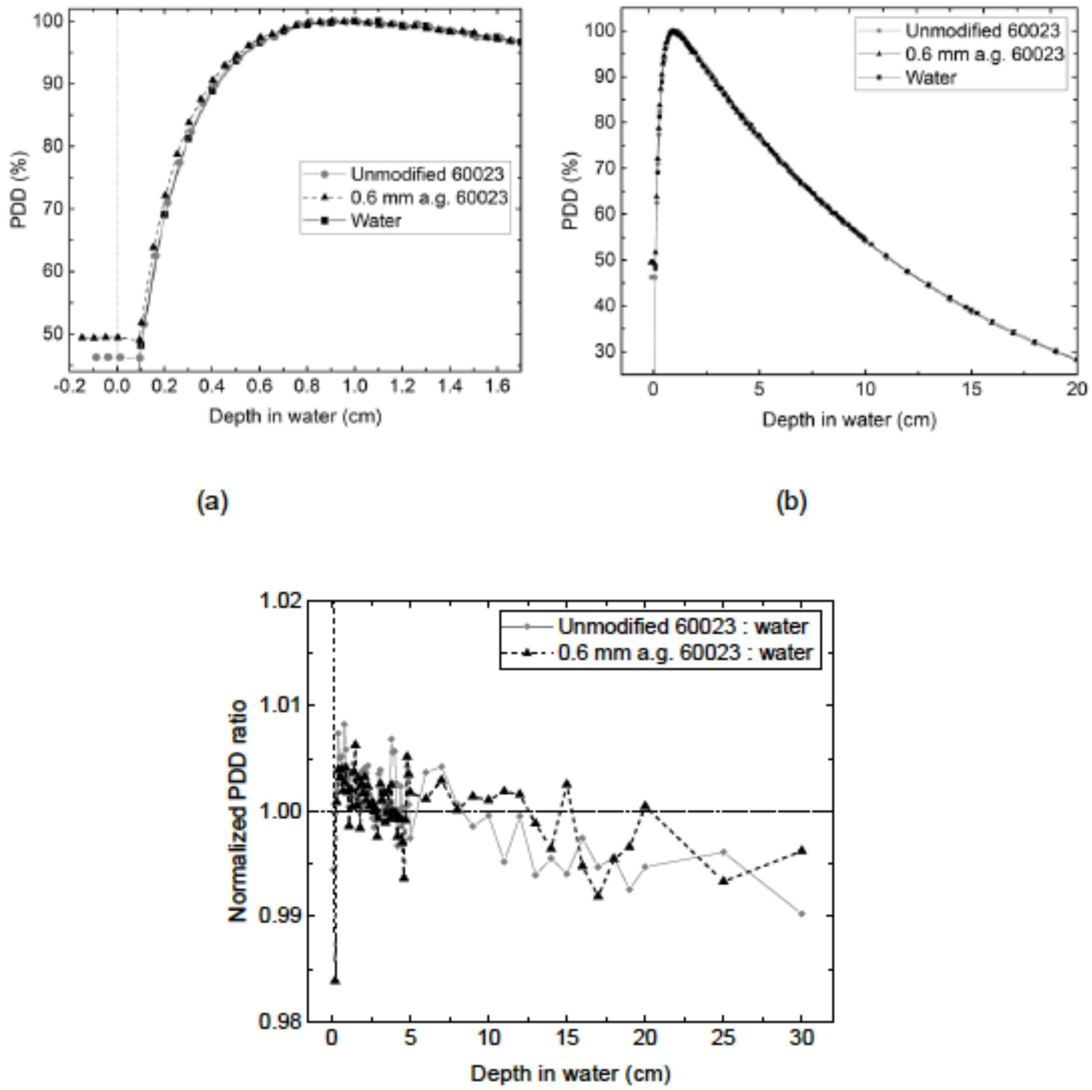
PDD (%)
Depth in water (cm)
Unmodified 60023
0.6 mm a.g. 60023
Water
Normalized PDD ratio
Unmodified 60023 : water
0.6 mm a.g. 60023 : water

(a) (b) (c)

FIG. 3.

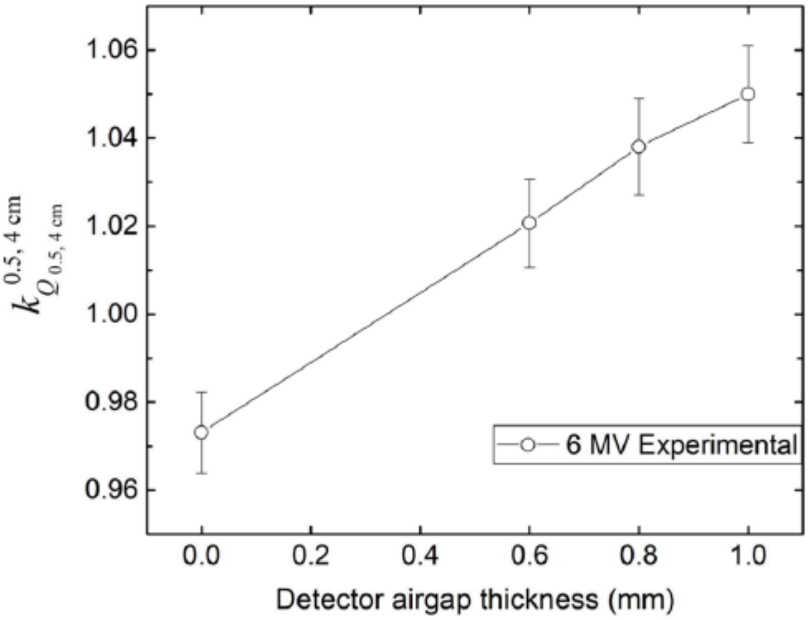

$k_{Q_{0.5,\,4\,\mathrm{cm}}}^{0.5,\,4\,\mathrm{cm}}$
1.06
1.04
1.02
1.00
0.98
0.96
0.0
0.2
0.4
0.6
0.8
1.0
Detector airgap thickness (mm)
6 MV Experimental

FIG. 4.

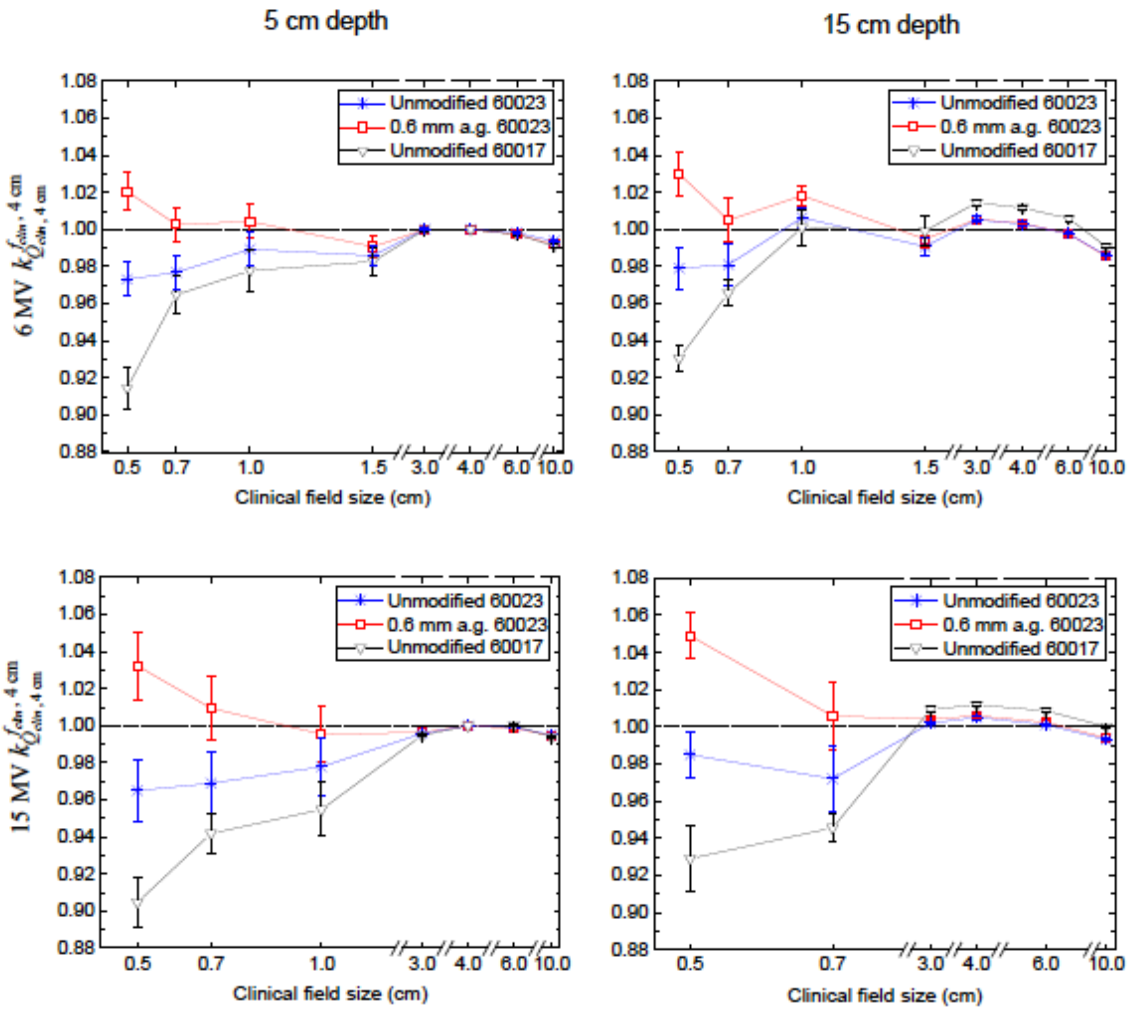
5 cm depth
15 cm depth
Unmodified 60023
0.6 mm a.g. 60023
Unmodified 60017
6 MV $k_{Q_{clin},Q_{msr}}^{f_{clin},4\ cm}$
15 MV $k_{Q_{clin},Q_{msr}}^{f_{clin},4\ cm}$
Clinical field size (cm)
1.08
1.06
1.04
1.02
1.00
0.98
0.96
0.94
0.92
0.90
0.88
0.5
0.7
1.0
1.5
3.0
4.0
6.0
10.0

FIG. 5.

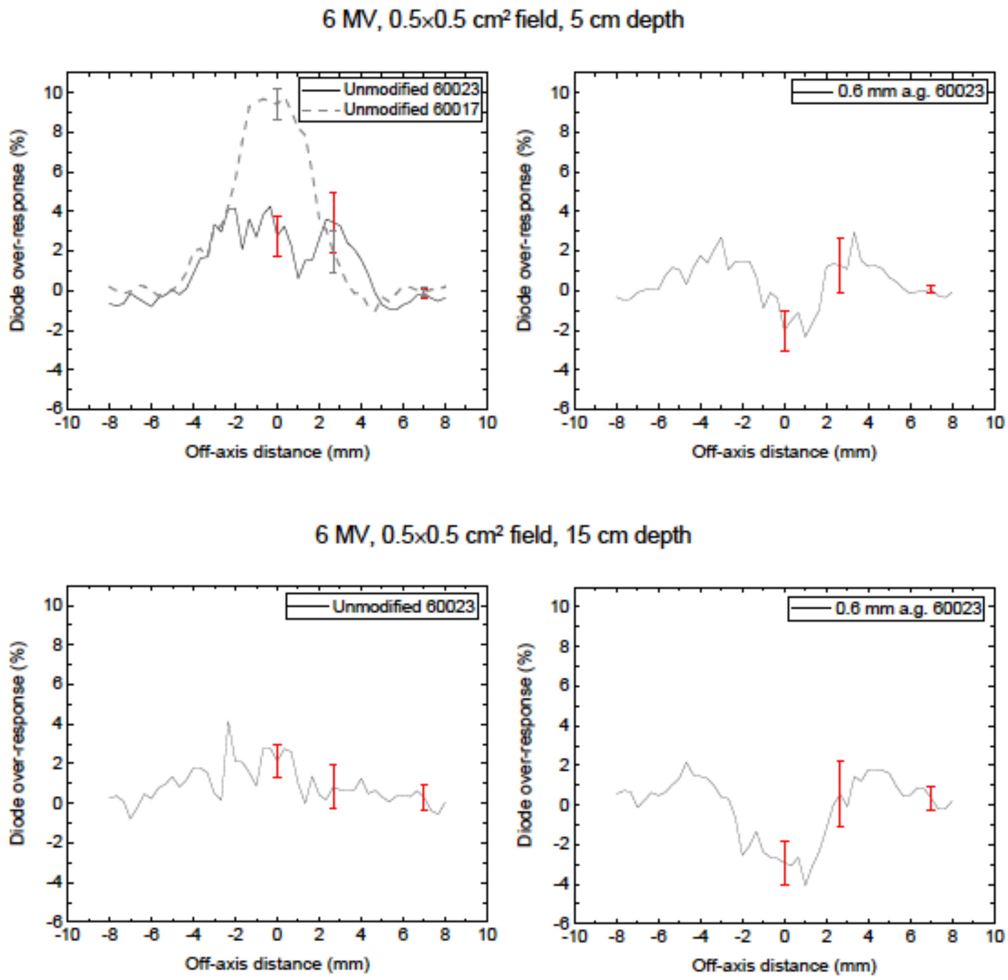
6 MV, 0.5×0.5 cm² field, 5 cm depth
Unmodified 60023
Unmodified 60017
0.6 mm a.g. 60023
Diode over-response (%)
Off-axis distance (mm)
6 MV, 0.5×0.5 cm² field, 15 cm depth
Unmodified 60023
0.6 mm a.g. 60023
Diode over-response (%)
Off-axis distance (mm)

FIG. 6.

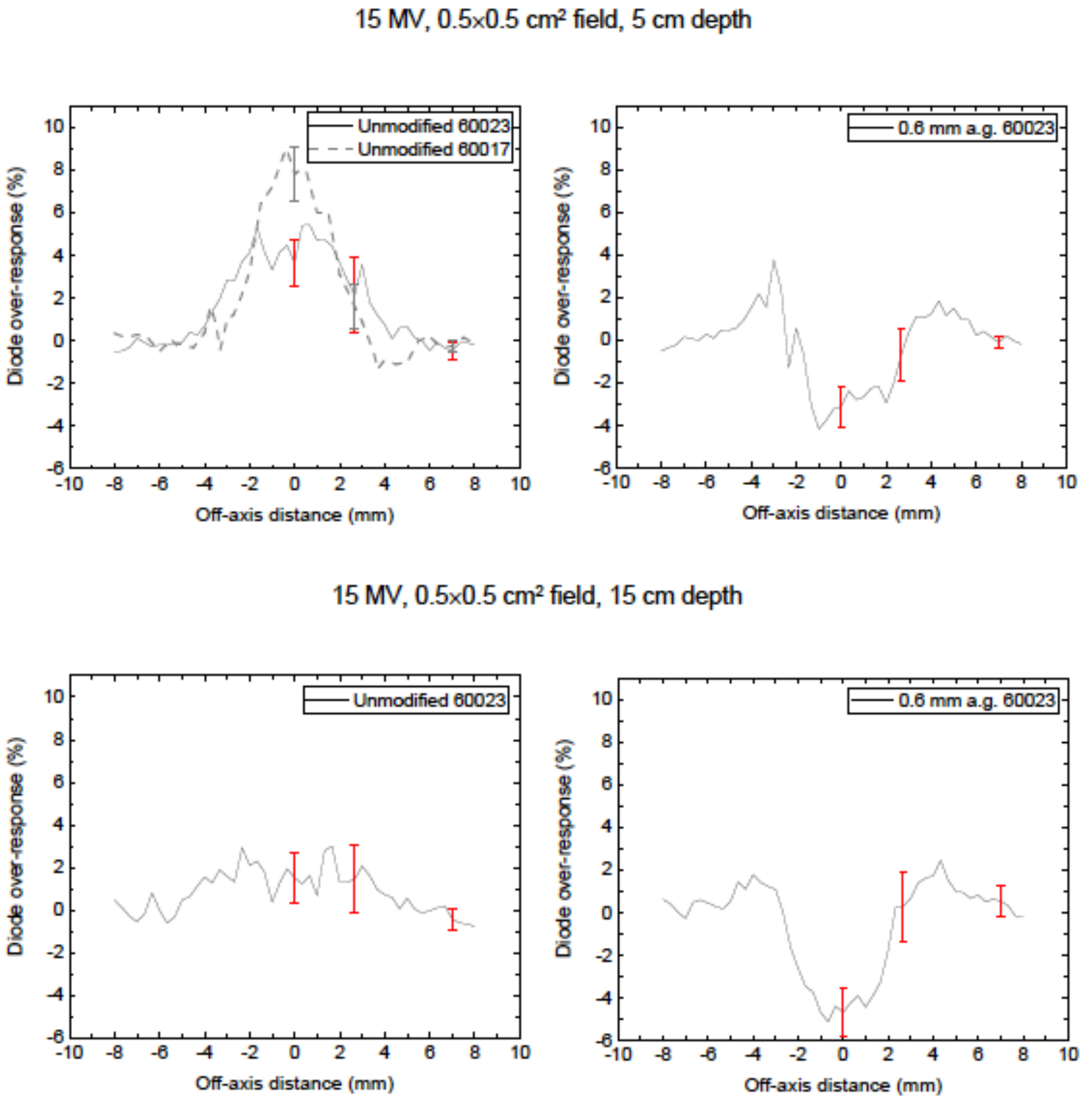
15 MV, 0.5×0.5 cm² field, 5 cm depth
Unmodified 60023
Unmodified 60017
0.6 mm a.g. 60023
15 MV, 0.5×0.5 cm² field, 15 cm depth
Unmodified 60023
0.6 mm a.g. 60023
Diode over-response (%)
Off-axis distance (mm)

FIG. 7.

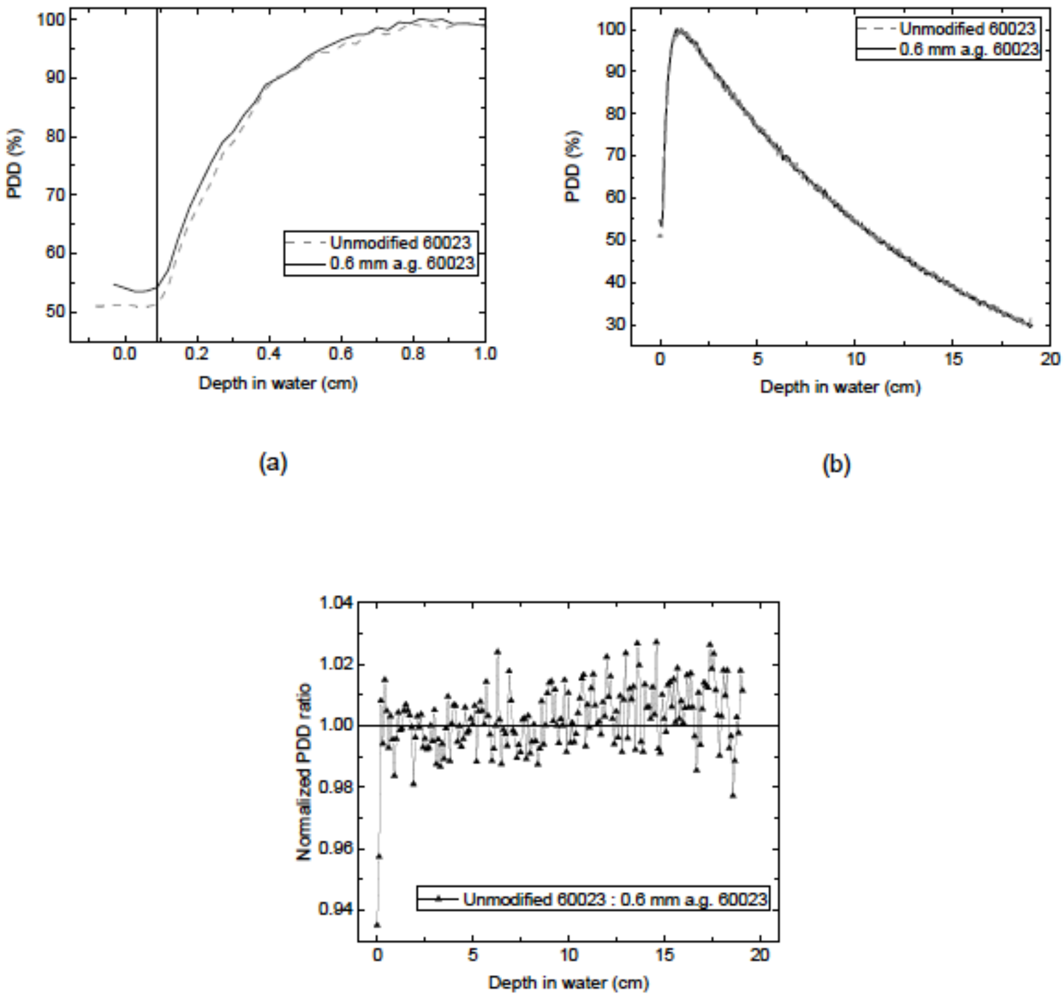

PDD (%)
Depth in water (cm)
Unmodified 60023
0.6 mm a.g. 60023
(a)
PDD (%)
Depth in water (cm)
Unmodified 60023
0.6 mm a.g. 60023
(b)
Normalized PDD ratio
Depth in water (cm)
Unmodified 60023 : 0.6 mm a.g. 60023

653

FIG. 8.

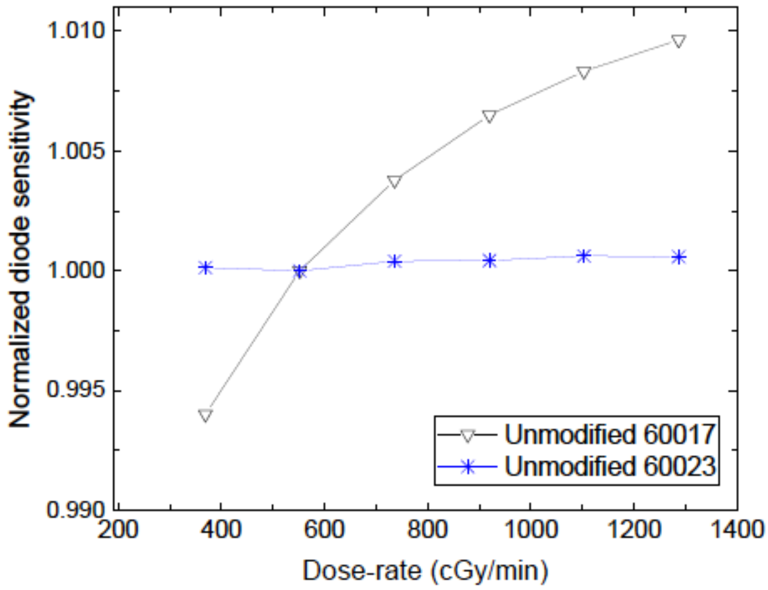
1.010
1.005
1.000
0.995
0.990
Normalized diode sensitivity
200
400
600
800
1000
1200
1400
Dose-rate (cGy/min)
Unmodified 60017
Unmodified 60023

TABLE I. Voxel dimensions used in Monte Carlo calculations of doses absorbed by water. The first two voxel dimensions listed are perpendicular to the beam axis, the third along it. Levels of precision achieved in dose calculations are also shown as ± 2 standard deviation (s.d.) uncertainties.

Field size (mm^2)	5×5	7×7	40×40	
Voxel location	**Voxel dimensions (mm^3)**			**Dosimetric precision (%)**
On-axis 5 & 15 cm depth	0.25×0.25×0.5	0.25×0.25×0.5	2×2×0.5	± 0.5
Off-axis	0.25×0.25×0.5	–	–	± 1.1
PDD up to 10 cm depth	0.25×0.25×1.0	–	–	± 0.4
PDD 10-30 cm depth	0.25×0.25×10.0	–	–	± 0.4

TABLE II. Monte Carlo $k_{Q_{clin,4\ \mathrm{cm}}}^{f_{clin},4\ \mathrm{cm}}$ factors calculated on-axis in 6 and 15 MV beams for unmodified 60017- and 60023-type detectors, and for 60023-type detectors modified to include 0.6 mm and hypothetical 0.3 mm airgaps. ± 2 s.d. confidence intervals are shown.

Detector model	Airgap thickness (mm)	6 MV $\boldsymbol{k_{Q_{0.5,4\ \mathrm{cm}}}^{0.5,4\ \mathrm{cm}}}$	6 MV $\boldsymbol{k_{Q_{0.5,4\ \mathrm{cm}}}^{0.7,4\ \mathrm{cm}}}$	15 MV $\boldsymbol{k_{Q_{0.5,4\ \mathrm{cm}}}^{0.5,4\ \mathrm{cm}}}$	15 MV $\boldsymbol{k_{Q_{0.5,4\ \mathrm{cm}}}^{0.7,4\ \mathrm{cm}}}$
			5 cm depth in water		
60017	0	0.910 ± 0.005	0.971 ± 0.007	0.896 ± 0.005	0.959 ± 0.009
60023	0	0.979 ± 0.006	0.977 ± 0.006	0.978 ± 0.007	0.984 ± 0.007
60023	0.3	1.007 ± 0.006	0.995 ± 0.006	1.009 ± 0.007	1.003 ± 0.007
60023	0.6	1.029 ± 0.006	1.002 ± 0.006	1.041 ± 0.007	1.020 ± 0.007
			15 cm depth in water		
60017	0	0.913 ± 0.005	0.967 ± 0.009	0.900 ± 0.005	0.958 ± 0.009
60023	0	0.987 ± 0.008	0.988 ± 0.007	0.985 ± 0.008	0.984 ± 0.008
60023	0.3	1.010 ± 0.008	1.007 ± 0.008	1.013 ± 0.008	1.002 ± 0.008
60023	0.6	1.038 ± 0.008	1.012 ± 0.008	1.043 ± 0.008	1.017 ± 0.008

TABLE III. Ratios of readings at 15 and 5 cm depths in water on-axis in a 6 MV 4×4 cm^2 field. ± 2 s.d. confidence intervals are shown. Ratios are shown for different detectors in the centre column, while the right-hand column shows how these ratios compare to that measured using the ionization chamber.

Detector	Ratio of readings at 15 and 5 cm depths	Detector ratio / ionization chamber ratio
IBA CC13 ionization chamber	0.540 ± 0.001	-
PTW 60017-type diode	0.534 ± 0.001	0.989 ± 0.002
PTW 60023-type diode (no airgap)	0.538 ± 0.001	0.997 ± 0.002
PTW 60023-type diode (0.6 mm airgap)	0.538 ± 0.001	0.997 ± 0.002